Towards an optimum design of wave energy converter arrays through an integrated approach of the life cycle performance and operational capacity

Alejandro López-Ruiz[a,*], Rafael J. Bergillos[b], Juan M. Raffo-Caballero[a], Miguel Ortega-Sánchez[b]

[a]*Departamento de Ingeniería Aeroespacial y Mecánica de Fluidos, Universidad de Sevilla, Camino de los Descubrimientos s/n, 41092, Sevilla, Spain*
[b]*Andalusian Institute for Earth System Research, University of Granada, Avda. del Mediterráneo, s/n, 18006, Granada, Spain*

Abstract

Over the last decades, several efforts have been made to develop an alternative and sustainable energy source from wind waves. To achieve the financial sustainability of this technology, most of the research has focused on analyzing facilities composed by several wave energy converters (WECs) arrays instead of isolated ones. Although the interaction between devices and its implications on the performance of the facilities have been studied beforehand, these previous works only considered certain combinations of sea states, limiting the applicability of the results. This work applies a new methodology based on statistical methods to assess the performance of different WEC array distributions during their entire life-cycle in an efficient way, using downscaling techniques and advanced numerical modeling for the propagation of the wave climate. The results obtained during the hindcasted life-cycle are used to analyze the maintenance and operation capabilities of the different alternatives of arrays defined for the WEC facility. The interactions between devices and their efficiency considering the associated impact are also quantified. The whole process was applied to a hypothetical array location in the Gulf of Cádiz (southwestern Spain), where three different array distributions were defined. Results show that the distance between WECs is a key parameter that controls the potential energy production, the efficiency

*Corresponding author
alopez50@us.es

of the facility and the interaction between several devices.

Keywords: Wave energy converters, array layout, performance, maintenance, hindcasting, downscaling

1. Introduction

During recent years, the development of non-conventional renewable energy technologies has received increasing attention due to the environmental problems derived from the use of fossil fuels. Among these non-conventional sources, marine energy is a kind of renewable energy source, which is stored in form of thermal, kinetic, chemical and biological energy (Khan et al., 2017). Accordingly, many recent works have focused on these types of sources, specially on the hydro-kinetic energy extraction. Two main technologies have been developed: (1) the extraction of energy from tidal currents using Tidal Energy Converters (TECs; Pacheco and Ferreira, 2016) and (2) the extraction of energy from waves through the use of Wave Energy Converters (WECs; López-Ruiz et al., 2016).

WECs generate electricity from the kinetic energy of waves by means of different physical processes, such as wave overtopping, wave impact or wave oscillation (López et al., 2013). The devices can be placed at maritime infrastructures, in the nearshore or offshore, and usually have dimensions ranging from tens to hundreds of meters. In order to optimize the economical viability of this wave energy resource, the devices are not installed isolated but in arrays or farms of many units.

Numerous studies have focused on the interactions among nearby devices. The first ones analyzed very simple array geometries forced by unidirectional regular waves (Budal, 1977; Falnes, 1980). Later, research interest was focused on more complex design parameters: Babarit (2010) analyzed the interaction between two WECs and the influence of the separation between them; whereas Borgarino et al. (2012) presented a study on the interaction between WECs in arrays of 9 to 25 devices within a yearly scale. de Andrés et al. (2014) addressed the optimum array configurations, in terms of power production, for different wave climates around the globe. Engstrom et al. (2013) and Goteman et al. (2014) analyzed the fluctuations in power availability of different arrays configurations, minimizing the power variance for some wave conditions and array geometries. More recently, Bozzi et al. (2017) assessed

the performance of different WEC array geometries along the Italian offshore platform using some combinations of real sea states.

To the authors best knowledge, the performance of different alternatives of array distributions for complete wave climate time series, spanning the entire life-cycle of the WECs, has not been implemented; with previous works analyzing only certain combinations of wave climate. This limits the information for the decision-makers, who usually have to make important investments in a technology where the commercial margins are narrow.

The main objective of this work is to assess the potential life-cycle performance of different geometrical configurations of WEC arrays using hincasted wave climate. The methodology, which will be described throughout the manuscript, can be divided into two main stages: (1) the definition of the WEC array configuration and (2) the evaluation of its performance using a numerical model. Furthermore, cutting-edge statistical methods are applied in order to obtain the wave energy potential for every individual WEC during its life-cycle with a minimum computational cost. The methodology is used to evaluate 9 different array configurations of 9–WEC devices in the southwestern coast of Spain. Results are obtained for a set of 25–year hindcasted wave data. The different alternatives are evaluated not only in terms of energy production, but also in terms of their environmental impact (i.e. occupied surface), and operational and maintenance aspects.

2. Study site

The southwestern area of the Gulf of Cádiz is one of the few locations along the southern coast of Spain where it is feasible to install a WEC array due to its wide continental shelf (30 km), relatively low depths and mild slopes (Ortega-Sánchez et al., 2008), with the shelf-break at approximately 120 m water depth (Fig. 1a-b). In addition, there is a strong wave energy potential in this area (Reikard et al., 2016). These characteristics enhance the feasibility of exploiting the wave energy resource according to the guidelines of the Kyoto protocol and the European Union and Spanish energy politics (Besio and Losada, 2008). In this work, the WEC arrays were placed at the widest part of the inner continental shelf, close to Trafalgar Cape, so that the arrays operate in intermediate depths (approximately 34 m) but at a considerable distance from the coast ($\simeq$ 10 km). This location is feasible

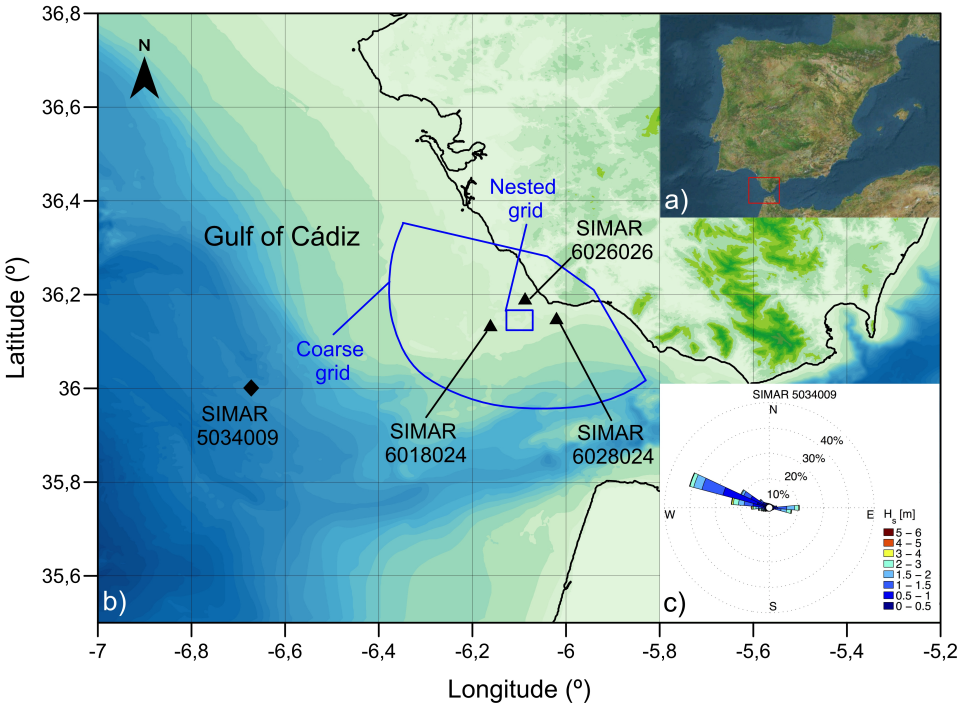

Figure 1: a) Location of the study site (Gulf of Cádiz, southwestern Spain); b) delimitation of the area where the WEC arrays were placed (small blue polygon), boundaries of the grids used in the numerical model (blue polygons), and location of the point in which wave data were available (black squares and triangles); c) wave rose based on the SIMAR 5034009 data.

in terms of economical exploitation (Iglesias and Carballo, 2014; Abanades et al., 2015), and it minimizes the environmental impact of the facility.

The area is a mesotidal and swell-dominated coastal environment. The astronomical tide is semi-diurnal with tidal ranges between 1.2 m and 3.8 m (Ortega-Sánchez et al., 2008). Wave data from SIMAR point 5034009 indicate that the prevailing incoming wave directions are west and west-northwest (Fig. 1c). The 50%, 90% and 99% exceedance significant wave heights (H_s) in deep water are 1.1 m, 2.2 m and 4.0 m, respectively. During extreme storms, maximum significant wave heights typically exceed 3.5 m.

3. Methodology

The methodology applied to hindcast the performance of different WEC arrays geometries in the study site is described in the following sections. Furthermore, we present the tools used to analyze the results, including the procedure to evaluate the relative impact of the different array layouts.

3.1. Wave climate

The main objective of this work is to obtain the performance of WEC arrays during their life-cycle, which is usually considered to be of 25 years (Margheritini et al., 2009; Alonso et al., 2015). Hence, we gathered wave dataset spanning 25 years obtained from the hindcasted database of Puertos del Estado (Spanish Ministry of Public Works).

We used hindcasted synthetic wave data obtained at 4 different locations (Fig. 1b). They correspond to nodes of a computational mesh with a resolution of approximately 1° in which data every 3 hours are available. These wind and wave data are obtained through the High Resolution Limited Area Model (HIRLAM, Cats and Wolters, 1996), and the WAM model (Booij et al., 1999), respectively.

SIMAR points 6018024, 6026026 and 6028024 correspond to intermediate depths and were used to calibrate the wave propagation model, as described in Section 3.2. These datasets spanned 11 years from 2005 to 2016. SIMAR 6018024 data was also used to define the orientation of the WEC arrays (Section 3.3.2). On the other hand, SIMAR 5034009 corresponds to deep-water data spanning 58 years from 1958 to 2016. Given its length, this dataset was used to obtain the hindcasted database of sea states to be propagated with the numerical model by means of downscaling techniques, and also to obtain the 25-year wave climate series.

In terms of computational effort and efficiency, the use of 25-year wave climate time series for the assessment of energy resource is a challenging task. The propagation of the complete dataset would involve a vast number of cases in the numerical model, which would limit the applicability of the presented methodology. To reduce this computational effort, statistical tools were applied through the use of downscaling techniques previously validated for the Mediterranean coast of southern Spain by Bergillos et al. (2016) and López-Ruiz et al. (2016).

Firstly, a database of representative wave conditions (H_s, T_p and θ_m) is generated applying the downscaling method presented by Camus et al. (2011, 2014) to the SIMAR 5034009 data. This first step synthesizes the total dataset of deep-water wave climate in a reduced number of sea states (300 in this case) representing mild, mean and extreme wave conditions not equally distributed and accounting for the most likely sea states. Secondly, this database is propagated using the wave propagation model described in Section 3.2. By means of these propagations, nearshore wave parameters are obtained and used to compute the wave power P for every sea state of the database. Finally, with these results, the complete 25-year series of P are calculated for every WEC and array geometry through interpolation.

3.2. Numerical modeling

Waves were numerically propagated using the SWAN model, which was designed to simulate random, short-crested waves in coastal regions (Booij et al., 1999). The main processes included in the model are refraction due to bottom and current variations; shoaling, blocking, and reflections due to opposing currents; transmission/blockage through/by obstacles; wind effects; whitecapping; depth-induced wave breaking; bottom friction; and non-linear wave-wave interactions.

Thus, the model is able to simulate the effects of obstacles on the wave propagation patterns. These obstacles must have at least one mesh length in any of their dimensions to modify wave properties between adjacent grid points. This limits the minimum refinement for the numerical grids, although in this case the limiting factor was the capability of precisely capturing the effects of the obstacles. The effects on wave propagation are three: they reduce the wave height of waves propagating behind or over the obstacle all along its length, it reflects waves that impinge the obstacle, and it diffracts waves around its boundaries (Rusu and Guedes Soares, 2013). In the present work a specular reflection was implemented that implies constant reflection and transmission coefficients along the devices.

The model domain consists of two different grids, as shown in Fig. (1). The first is a coarse curvilinear 163x163-cell grid, with cell sizes of approximately 400x400 m. The second is a nested grid covering the area in which the WEC arrays were placed with 244x244 cells and cell sizes of about 15x15 m. For the spectral resolution of the frequency space, 37 logarithmically-distributed frequencies ranging from 0.03 to 1 Hz were used; whereas for

the directional space, 72 directions covering 360° in increments of 5° were defined.

The model was run in its stationary mode and was calibrated considering the following physical processes: refraction, white-capping, depth-induced breaking ($\alpha = 1$, $\gamma = 0.73$), nonlinear triad interactions ($\alpha = 0.1$, $\beta = 2.2$), bottom friction (Type *Collins*, coefficient=0.02) and diffraction (smoothing coefficient=0.6, smoothing steps=600). Similar values were obtained for similar applications in the nearby Bay of Cádiz (Zarzuelo et al., 2015). The calibration was performed comparing the model results with the SIMAR points 6018024, 6026026 and 6028028 data (Fig. 1) for the same locations. The calibration period spanned one month starting on September 1st, 2016, and the correlation coefficients (R^2) obtained were higher than 0.87 proving the validity of the defined numerical scheme.

3.3. WEC array layouts

3.3.1. Modeling individual WECs

This work focuses on floating overtopping WECs, which use a sloping plate that leads the waves to overtop into a reservoir located immediately behind it. The energy is extracted by means of low head turbines, using the difference in water levels between the reservoir and the average sea water level (Vicinanza et al., 2012). Specifically, we applied the methodology to the WaveCat prototype device (Fernandez et al., 2012; Allen et al., 2016). This overtopping WEC has an overall width of $D \simeq 100$ m, and is moored in a single point to the seabed, orientating itself along the direction of wave propagation passively (Allen et al., 2016).

The WECs were included in SWAN as obstacles with circular shape, so that the devices always expose the same width to the incident waves, regardless of the incoming wave direction, simulating the self-orientation behavior of the device. As described in Section 3.2, SWAN requires the definition of reflection and transmission coefficients to account for the effect of the presence of obstacles. These coefficients are partially confidential due to commercial reasons, but in the case of the WaveCat WECs, Fernandez et al. (2012) presented values obtained from experimental tests. Although different results were obtained depending on the wave conditions (variations lower than 10%), based on the results of these tests, we adopted constant mean values of $k_t = 0.75$ and $k_r = 0.44$ for the transmission and reflection coefficients, respectively. Fig. (2) shows six examples of the results obtained using these

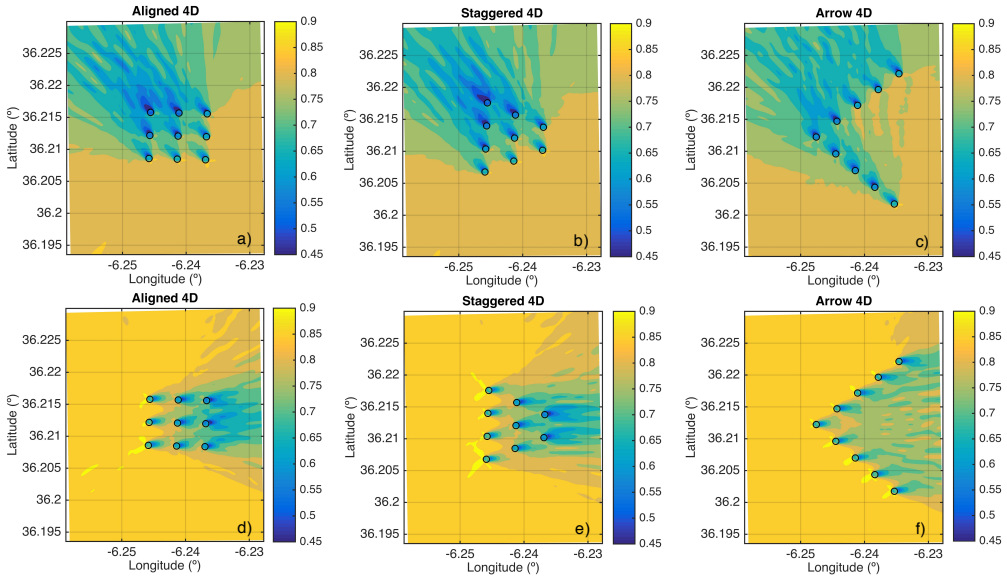

Figure 2: Propagation coefficients (relation between deep-water and local wave heights) for the *Aligned* (left panels), *Staggered* (central panels) and *Arrow* (right panels) geometries under southeasterly (upper panels) and westerly (lower panels) waves with $H = 3.4$ m and $H = 6.1$ m, and $T = 10.8$ s and $T = 11.3$ s, respectively. These sea states correspond to cases 275 and 298 of the defined database.

coefficients for two sea states and three array layouts. The effects of the obstacles on the wave height distribution are clearly observed.

3.3.2. WEC arrays

Four variables define the geometrical layouts of WEC arrays: (1) the number of devices, N, (2) the shape of the array, (3) the distance between WECs, W, and (4) the orientation of the array. In this paper, arrays of $N = 9$ and distances between WECs of $W = 2D$, $4D$ and $6D$ were defined, according to previous works (Bozzi et al., 2017; Mercadé Ruiz et al., 2017). Furthermore, three different shapes of WEC arrays were considered (Fig. 3): (1) regular array of 3x3 elements (*Aligned*), (2) staggered shape in three columns of 4, 3 and 2 devices, trying to minimize the effect of the wave trail generated for the outer devices (*Staggered*), and (3) arrow shape, trying to avoid shadowing effects between WECs (*Arrow*). Thus, a total of 9 layouts with 9 WECs each were tested.

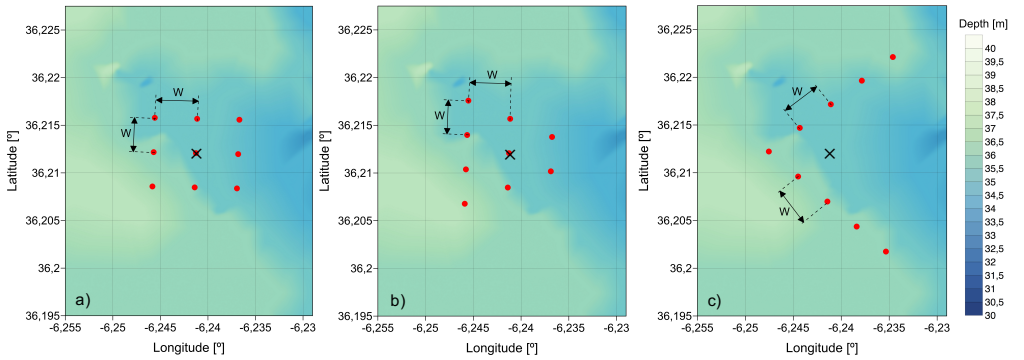

Figure 3: Shape of the WEC arrays defined: a) *Aligned*, b) *Staggered*, and c) *Arrow*. W represents the separation between WECs. The examples depicted correspond to $W = 4D$. The black crosses indicate the geometrical center of the layouts.

The arrays were oriented to the main incoming wave direction (in terms of wave energy). To obtain this direction, the wave energy resource P was obtained for the SIMAR point 6018024, which is the nearest to the location of the arrays (Fig. 1). The assessment of P is described in Section 3.4, and results are shown in Fig. (4). They reveal that the majority of the wave energy is provided by westerly waves. Hence, the three geometries were oriented to the west, as depicted in Fig. (3).

3.4. Assessment of the wave energy resource

The available wave energy resource was evaluated in terms of wave power per unit of wave crest length (P, in W/m). This was obtained from the spectral output of the wave propagation model as:

$$P = \rho g \int_0^{2\pi} \int_0^{\infty} S(f,\theta) c_g(f,h) df d\theta \tag{1}$$

where ρ is the water density, g is the acceleration of gravity, $S(f,\theta)$ is the directional wave spectrum, f is the frequency, θ is the propagation direction of the spectral component, c_g is the group celerity and h is the water depth. Eq. (1) can be approximated by (Besio et al., 2015):

$$P = \frac{1}{16} \rho g H_{m0}^2 c_g \tag{2}$$

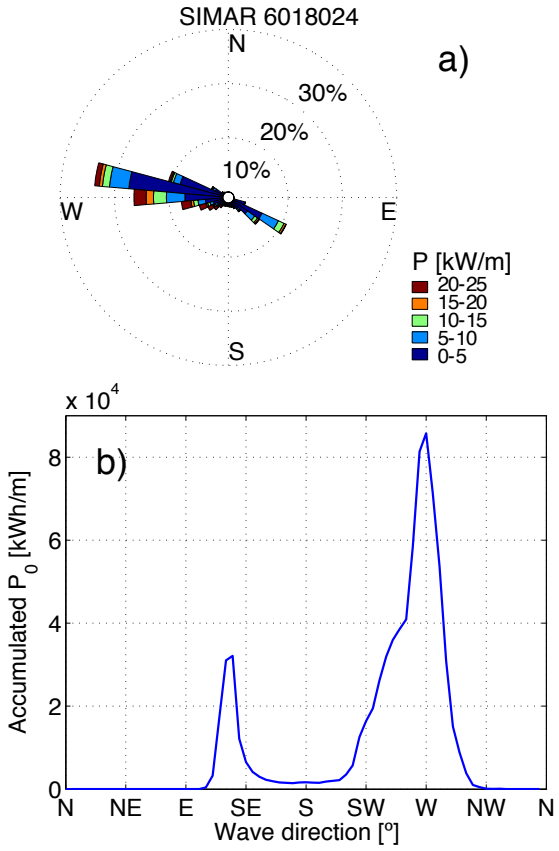

Figure 4: Wave energy resource (P) obtained for SIMAR point 6018024 data: a) P rose, and b) accumulated P as a function of the incoming wave direction.

where H_{m0} is the spectral wave height evaluated from the wave energy spectrum, whose spectral moments are defined as:

$$m_i = \int_0^{2\pi} \int_0^{\infty} S(f,\theta) f^i df d\theta \tag{3}$$

Thus, $H_{m0} = 4\sqrt{m_0}$ and the wave period used to obtain c_g is $T_{m-1,0} = m_{-1}/m_0$ (Veigas et al., 2014; Veigas and Iglesias, 2014; Besio et al., 2015).

3.5. Analysis of the results

Four main aspects of the WEC arrays were analyzed: (1) the performance of the different geometrical layouts in terms of potential energy production, (2) the interaction between WECs, which is positive (negative) if there is a power production gain (loss) compared with isolated systems, (3) the relative performance of the arrays, considering their impact in terms of occupied surface and maximum length in which waves are perturbed, and (4) the maintenance and operational possibilities. For that, 25 years of P were interpolated using the deep-water wave data of SIMAR 5034009 from January 1st, 1992 to December 31st, 2016.

For the first aspect, average, 95% percentile and standard deviation of P were obtained based on the hindcasted data. For the second, two different approaches were followed to quantify the interactions: (1) the assessment of the root mean square error (RMSE) and the correlation coefficient (R) between the individual performance of the WECs in an array and the performance of an isolated WEC, and (2) the assessment of the $q-$factor, defined as the ratio between the power output of an array of N WECs and the power output of N isolated WECs:

$$q = \frac{P_{\text{array}}}{N * P_{\text{isoWEC}}} \tag{4}$$

where P_{isoWEC} is the energy resource for an isolated WEC located at the geometrical center of the array (Fig. 3). This was adopted because depth variations across the zone are lower than 10%, so that P variations between isolated WECs at different places inside the zone are negligible.

For the third aspect, two parameters were used to quantify the impact: the surface occupied by the facility (S_f), defined as the area inside the envelope of the WECs (Fig. 3), and the maximum width of the facility that opposes incoming waves (W_f). With these parameters, the P per unit of

S_f (P_S) and W_f (P_W) were assessed to analyze the efficiency of each array configuration in terms of environmental and visual impacts.

In the case of the operation and maintenance of the WECs, a similar approach to that presented by López-Ruiz et al. (2016) was adopted, analyzing four different parameters. First, the availability defined as the percentage of time in which the WECs are able to produce electricity with local wave conditions, considering the range of operational wave conditions of the particular devices installed. The second is the accessibility, which is the percentage of time in which the device could be accessed for maintenance tasks. This factor depends on the meteorological and wave conditions, and the type of WEC and vessels used (Guanche et al., 2014). The third parameter is the mean monthly number of weather windows (wws) of a certain duration, which are necessary to repair and maintain the WECs. These intervals include the travel time, which shortens the effective work time. Lastly, we computed the waiting period (wp), which is defined as the time interval between wws of a certain duration. Therefore, this factor accounts for the mean time that the maintenance workers have to wait until the weather conditions are suitable for a repair activity of a certain duration.

4. Results

4.1. Energetics performance of the array layouts

The mean, 95th percentile and standard deviation of P for the 9 array layouts are shown in Fig. (5). The three curves show similar trends: for the same array shape, P increases with increasing distance between arrays. Variations between layouts of the same shape are more evident for the *Aligned* and *Staggered* arrays, with differences up to 20% for the mean P in the case of the *Aligned* array. Differences between layouts of the same shape are much smaller for the *Arrow* array, with variations between $W = 4D$ and $W = 6D$ being almost negligible ($< 1\%$). These results highlight that the performance is lower as the distance between WECs decreases. Moreover, the performance of the *Arrow* is significantly higher than the other two geometries due to the lower shadowing effects between WECs (Fig. 5).

Fig. (6) depicts the mean P for the 25-year life-cycle for each array. The tendencies are again very similar for the *Aligned* (Fig. 6a-c) and *Staggered* (Fig. 6d-f) shapes: P is higher for the WECs located in the western column due to their higher exposure to more energetic sea states (Fig. 4). The mean

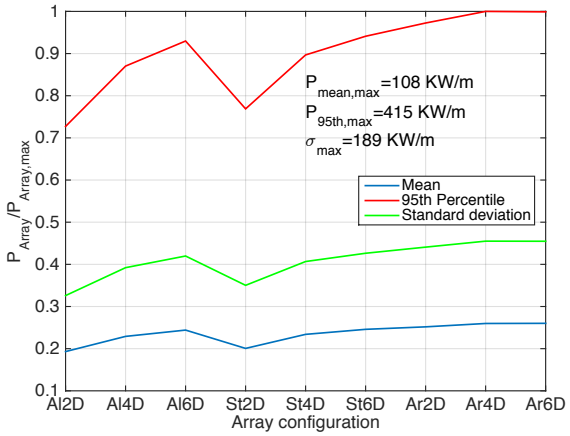

Figure 5: Mean (blue), 95th percentile (red) and standard deviation (green) of P for the 9 array layouts during the life-cycle period between 1992 and 2016.

P decreases to the east with no significant differences between WECs located in the same column.

For the *Arrow* shape, results indicate that the north wing of the *Arrow* is potentially capable of extracting more energy from waves, with higher values of P. This is attributed to the sheltering effect that WECs on the south wing have on themselves under WNW and SE waves, which are of certain importance according to Fig. (4). On the contrary, WECs of the north wing do not interact between themselves. In any case, the differences between WECs for this shape are much lower than those for the other two geometries, as shown in Fig. (7). It is observed that the variability decreases with increasing distance between WECs, indicating that the interactions between WECs are less important. The variability for the *Arrow* layouts is considerably lower than in the other geometries.

4.2. Analysis of the interactions between WECs

To quantify the interactions between WECs, the root mean square error (RMSE) and the correlation coefficient (R) for the mean P between WECs in the array and an isolated WEC in the geometrical center of the array were obtained. The results indicate that the differences between the WECs in the arrays and the isolated ones are clearly greater for the *Aligned* and the *Staggered* shapes (Fig. 8), highlighting that the interactions between WECs

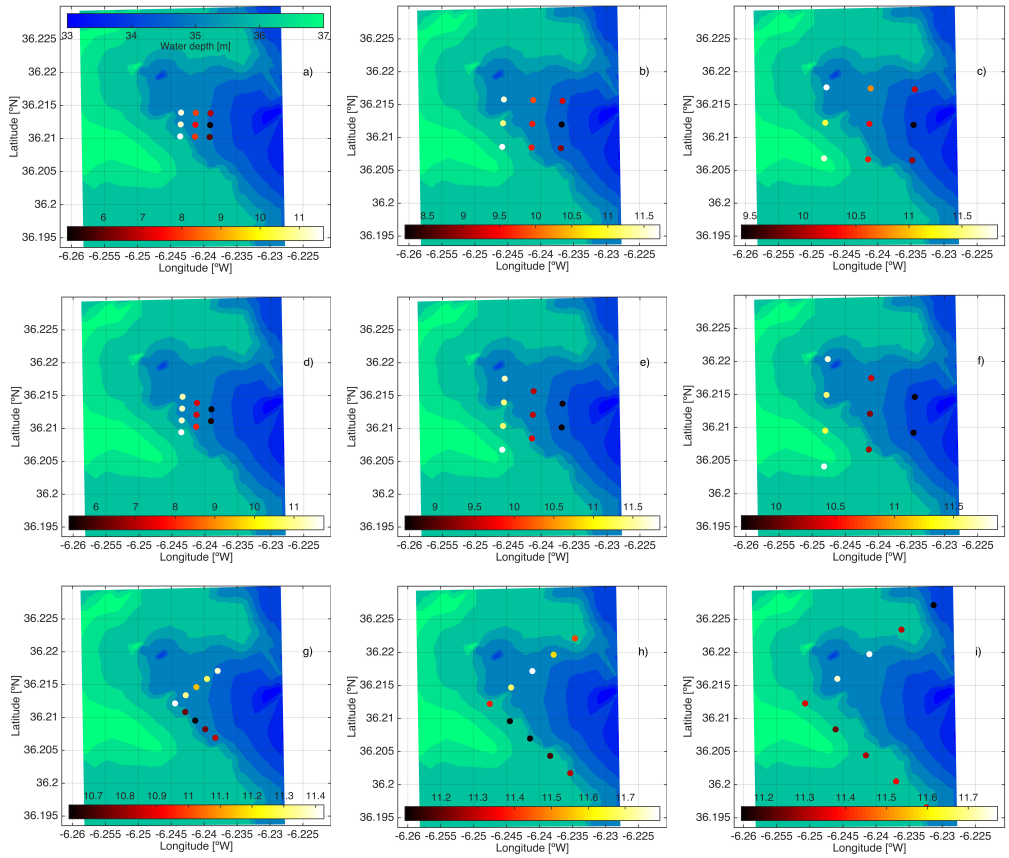

Figure 6: Mean P in kW/m obtained for every WEC of: a-c) *Aligned* arrays, d-f) *Staggered* arrays, g-i) *Arrow* arrays. Blue-green colormap indicates water depths, black to white colormap indicates mean P.

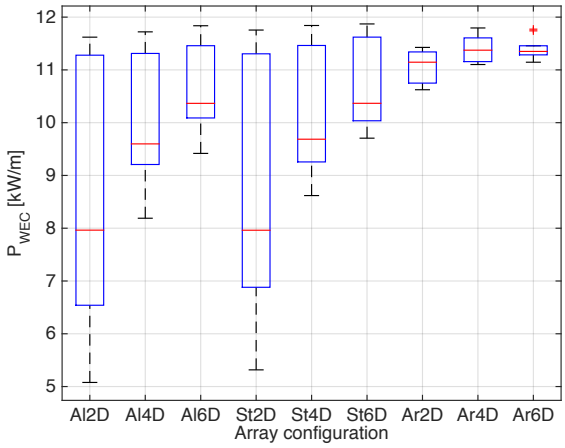

Figure 7: Statistical inference of the mean P obtained for the WECs of the different array configurations. In the boxplot, the central marks indicate the median and the edges of the box the 25th and 75th percentiles. Black crosses represent the extreme values.

are more important for these layouts. In the case of the *Aligned* geometry, WECs located at the west side of the layout present the lowest differences between the array and the isolated cases due to the predominance of W and SW waves. For the *Staggered* geometry, the correlations are improved with respect to the previous shape, since the west column of WECs (1 to 4) has one more device and also because the *Staggered* location of WECs in the central column (5 to 7) avoids the interaction with those of the west column. In the case of the *Arrow* geometry, R is below 0.997 only for the WECs 1 to 4 in the $2D$ layout. These WECs on the north wing of the *Arrow* are clearly affected by the prevailing direction of the most energetic waves (WSW sector, Fig. 4). Results show that a separation $W \geq 4D$ is enough to minimize these interactions. Finally, the RMSE decreases as W increases; whereas R increases with W, except for the WEC number 9 in the *Arrow* 6D layout.

RMSE and R provide insights into the differences between the values of P obtained for the arrays and those for an isolated WEC. However, they do not identify whether these differences lead to an increase in energy production compared to isolated WECs or not. To quantify that, the $q-$ factor was obtained for every array layout. Fig. (9) shows the statistical results for this factor obtained for each array layout at each WEC location. The $q-$factor is lower than 1 except for certain WECs in the case of the *Staggered* geometry,

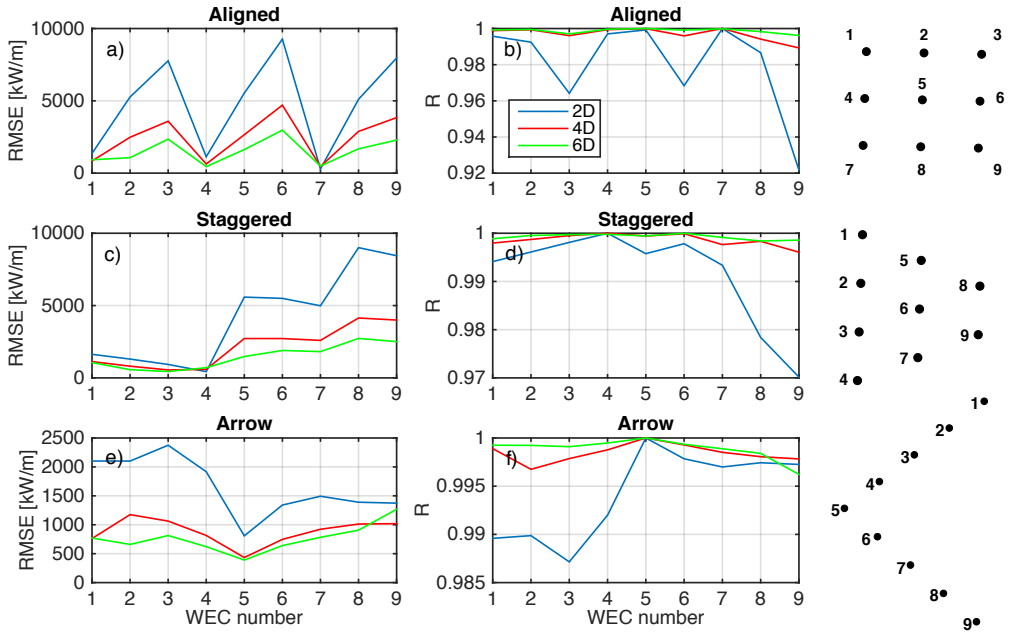

Figure 8: Root mean square error (RMSE) and correlation coefficient (R) between WECs in the arrays and an isolated WEC in the geometrical center of the array for the mean P: a-b) *Aligned*, c-d) *Staggered* and e-f) *Arrow*. Schemes at the right of the figure represent the position of each WEC.

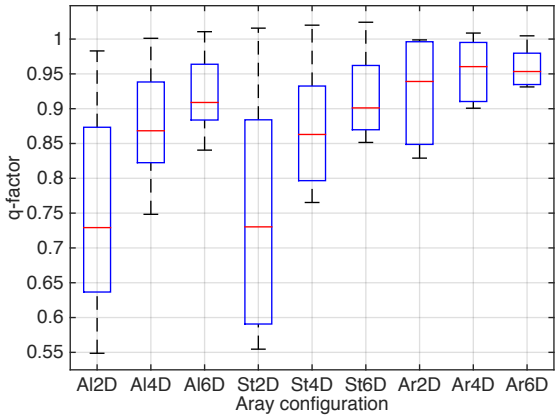

Figure 9: Statistical inference of the $q-$factor obtained for the WECs of each array configuration.

i.e., the interference between WECs is generally negative (an array of 9 WECs produces less energy than 9 isolated WECs). Moreover, the closer the WECs, the lower the $q-$factor, except for the case of the *Arrow* 6D layout. The variability of the $q-$factor for the same array layout also reduces as the distance between WECs decreases.

Fig. (10) depicts the mean $q-$factor obtained for the 25-year life cycle of the WECs. Differences between the *Arrow* geometry and the other two are evident: whereas minimum values are around 0.85 in the case of the *Arrow* layouts, they descend to 0.55 for the other two geometries for $W = 2D$. Positive interactions ($q > 1$) between WECs are found for one WEC and one value of W in the *Aligned* and *Staggered* geometries, whereas they are found for two WECs (3 and 4) in the case of the *Arrow* geometry. Regarding the distribution of the $q-$factor along the arrays, WECs located in the west column for *Aligned* and *Staggered* geometries are those with the highest $q-$factor, specially the WEC located more in the south. In the case of the *Arrow* geometry, the highest $q-$factor values were obtained for the north wing of the layouts.

4.3. Effectiveness of the array layouts

Fig. (11) shows the effectiveness of the different array distributions, considering the energy production per unit of occupied surface and facility width.

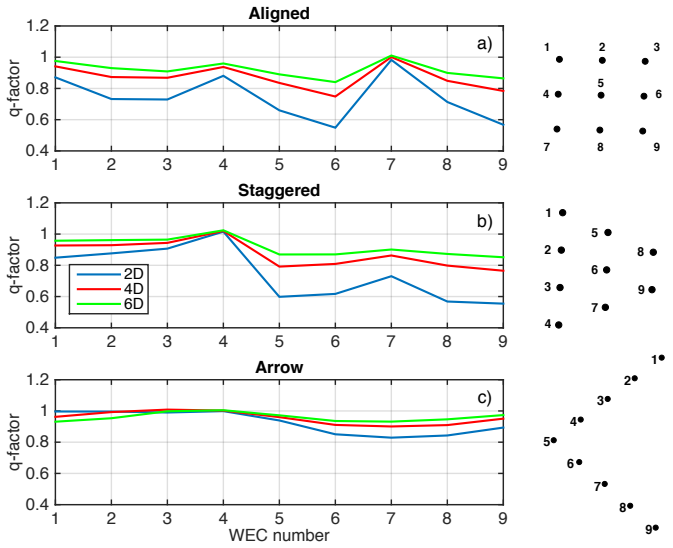

Figure 10: $q-$factor for the WECs locations for the 9 array layouts defined: *Aligned* (a), *Staggered* (b) and *Arrow* (c) geometries. Schemes in the right part of the figure represent the location of each WEC.

This effectiveness is quantified as the non-dimensional assessment of the energy resource to facilitate the comparison between array layouts. Results reveal that the percent variations in the effectiveness are significantly greater than those in the mean energy resource. As an example, the array layout with the minimum mean energy is only 25% lower than the one with the maximum value, whereas the minimum effectivenesses are 83% and 92% lower than the maximum values of P_W and P_S, respectively. The reduction of the effectiveness from $W = 2D$ to $W = 4D$ is greater than from $W = 4D$ to $W = 6D$, as exhibit the slopes of the green and red lines in Fig. (11).

4.4. Operational and maintenance aspects

4.4.1. Availability

The WECs are able to produce energy if the wave height at the entrance of the WEC ranges between minimum and maximum thresholds, which depend on the mechanical characteristics of the devices. In the case of the WaveCat WECs, there is no available information regarding this topic due to their early stage of development, so typical values for other types of WECs ($H_s \in [0.75, 5.9]$) were used (Guanche et al., 2014; López-Ruiz et al., 2016).

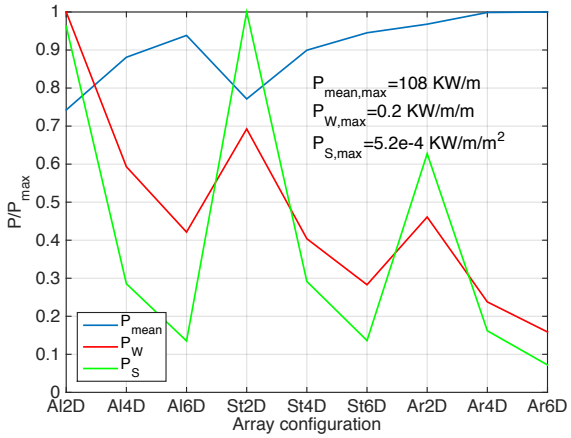

Figure 11: Non-dimensional mean P (blue line), P per unit of occupied wave front (P_W, red line), P per unit of occupied surface (P_S, green line) obtained for the life-cycle period of the WECs between 1992 and 2016.

Results depicted in Fig. (12) indicate that availability increases with higher distances between WECs, except for the case of the *Arrow* geometry, in which the higher availability is obtained for the intermediate W. Moreover, lower values are obtained for the WEC with lower energy performance, highlighting that the limiting factor for the availability is the lower threshold, i.e., the occurrence of low wave heights. Similar results were found for the *Aligned* and *Staggered* geometries, although contrary to the analysis of energy performance of the arrays, in this case the worst layout in terms of availability is the *Staggered* with $W = 2D$, where there are 4 WECs with availability lower than 40%.

On the other hand, the *Arrow* geometry presents higher availabilities and lower variabilities between devices, with values over 53% for every WEC and differences below 10% between the maximum and minimum availabilities in each layout. The maximum availability is almost equal for the 9 layouts defined. These maximum values correspond to the WECs less influenced by the presence of the other devices. Hence, the best geometry in terms of availability is the *Arrow*, in particular the array with $W = 4D$, for which the WECs are producing energy a large portion of the time.

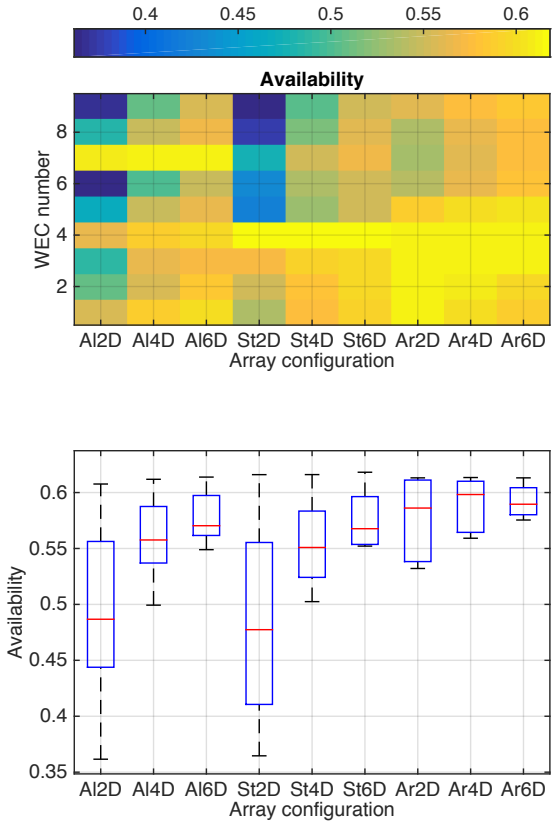

Figure 12: Availability (percentage of time during the life-cycle) obtained for the different WECs and array layouts. Upper panel depicts the mean availability for the life-cycle period for every WEC in each layout defined. Lower panel shows the statistical inference of these mean values.

4.4.2. Accessibility

In the case of the Gulf of Cádiz, considering the typical wave conditions and the vessels usually employed in the zone, a threshold of $H = 1.5$ m was used (Guanche et al., 2014). Although other variables such as the wind speed are also relevant for the accessibility, the wave height is the most limiting factor for the operationality of the vessels (López-Ruiz et al., 2016). Thus, this variable was adopted as the single variable defining accessibility.

Results show that the WECs with the lower accessibility are the ones for which the interactions between devices are less important (Fig. 13). In the case of the *Aligned* and *Staggered* geometries, they correspond to the west column of devices (1, 4, 7 and 1 to 4, respectively), presenting accessibilities of 82-85%. The major differences between WECs for these geometries are found for the layouts with $W = 2D$. Values up to 94% were obtained for the devices located at the northeast of the arrays, influenced by the sheltering effect of the other devices. The variability in the accessibility to the devices between WECs of the same layout is much lower for the *Arrow* geometry. Furthermore, median values of the WECs (red lines in the lower panel of Fig. (13) are lower than 83%.

4.4.3. Number of weather windows

For the mean monthly number of weather windows (wws hereinafter), periods of 6, 12 and 24 hours were considered. As well as in Guanche et al. (2014) and López-Ruiz et al. (2016), the number of consecutive periods of x hours wws has been considered. Thus, if there is a period of 48 h with accessible weather conditions, 8 wws of 6 h, 4 wws of 12 h and 4 wws of 24 h are obtained. During these periods, wave heights under 1.5 m were calculated in the vicinity of the devices, and a maintenance vessel would be able to approach the WECs to carry out repair or inspection tasks. However, since the vessels have to travel until the respective devices, the wave conditions in the surroundings of the facility must also be considered. To do that, the wave heights obtained for a scenario without arrays were used. Nevertheless, the possible trails of higher wave heights (see Fig. 2 for instance) were not considered, since it would require a special analysis of the vessel trajectories that is out of the scope of this work.

Results are shown in Fig. (14). The patterns in the number of wws are almost equal for the three periods considered and variations between WECs of different layouts are under 1%. Therefore, the limiting factor for the wws

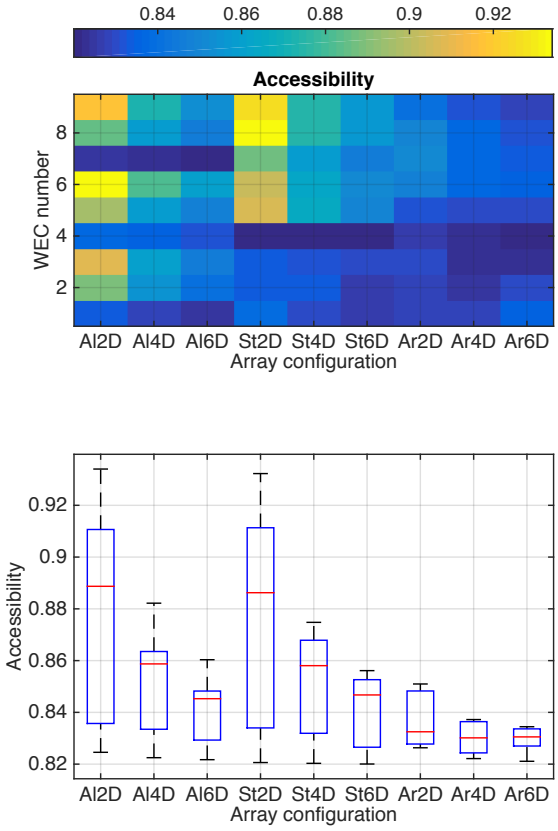

Figure 13: Accessibility obtained for the different WECs and array layouts. Upper panel depicts the mean accessibility for the life-cycle period for every WEC in each layout defined. Lower panel shows the statistical inference of these mean values.

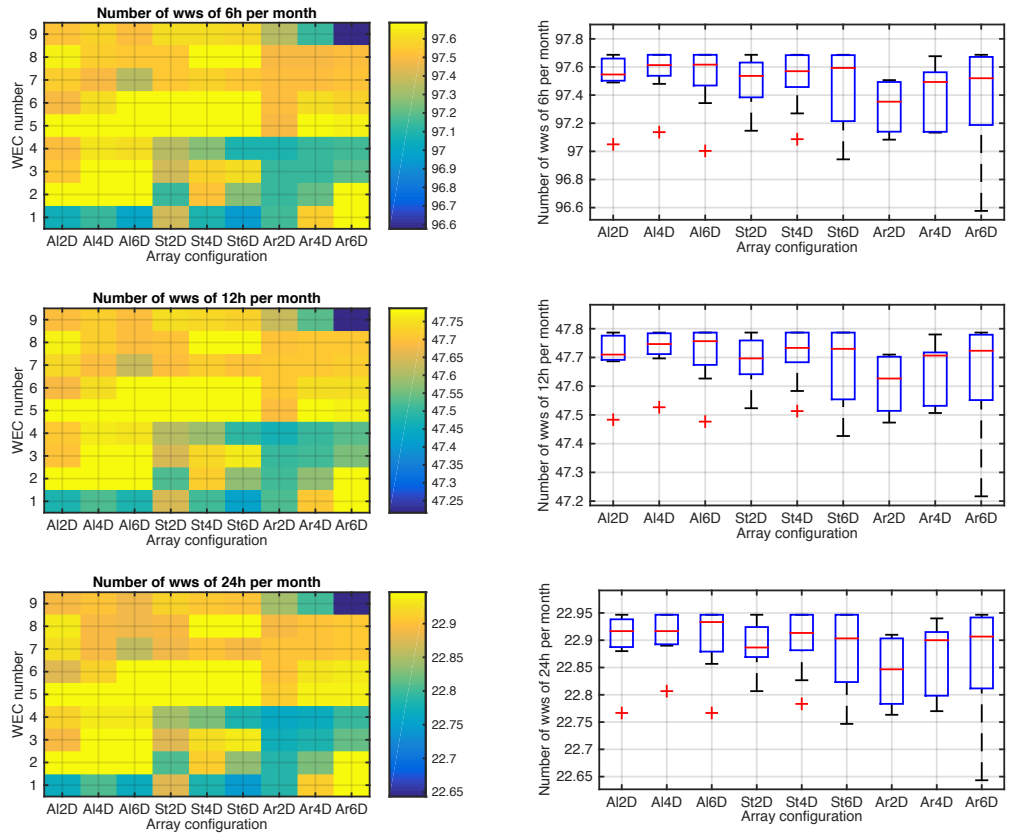

Figure 14: Mean monthly number of wws obtained for the different WECs and array layouts. Left panels depict the mean values for the life-cycle period for every WEC in each layout defined. Right panels show the statistical inference of these mean values.

are the wave conditions to travel until the facility instead of the conditions to approach the individual devices. For wws of 6 h, considering a mean number of wws of 97.1, approximately 83% of the possible wws are available to reach the devices, since a full mean month accessibility corresponds to 120 wws. This proportion reduces to 79% and 76% for wws of 12 and 24 h, respectively.

4.4.4. Waiting period

Periods of inaccessibility were also analyzed through the calculation of the waiting period (wp hereinafter) between wws. If a failure is detected in one or more devices and a maintenance task is required, it will only take place once the maintenance workers has an available wws to reach the WECs.

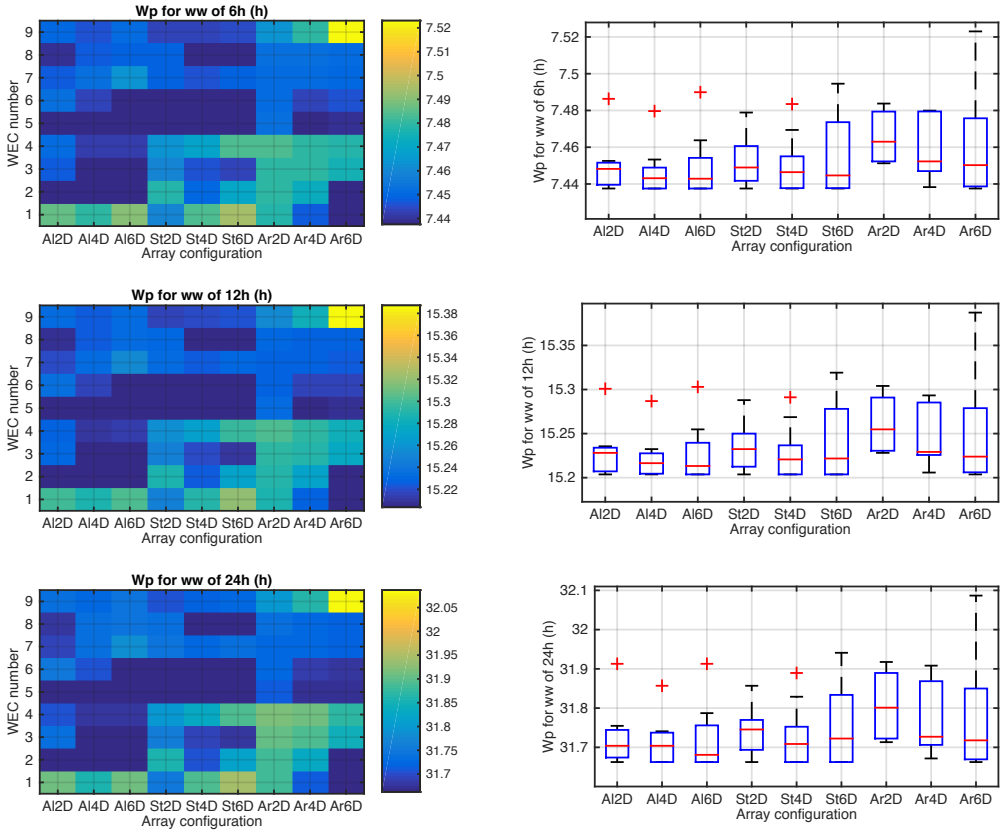

Figure 15: Mean wp obtained for 6, 12 and 24 h wws for the different WECs and array layouts. Left panels depict the mean values for the life-cycle period for every WEC in each layout defined. Right panels show the statistical inference of these mean values.

In this section, the definition of the wws is the same as in the previous one. Thus, conditions for both the travel until the facility and the approach to the WECs are considered.

Fig. (15) shows that the results are very similar to those of the number of wws. The average wp for wws of 6 h is around 7.48 h, whereas it increases up to 15.3 and 31.9 h for wws of 12 and 24 h, respectively. The variability between WECs is again under 1%, indicating that the wave conditions to travel until the facility are the limiting factor.

5. Conclusions and final remarks

Although the interactions between WEC devices and their implications on the performance of the facilities have received increasing attention during recent years, the issue has been generally addressed considering only certain combinations of sea states, reducing its applicability. In addition, the maintenance and operation capabilities of the WEC arrays have not been analyzed in detail. This paper assesses the performance of different geometrical configurations of WEC arrays during their entire life-cycle using statistical tools to reduce the computational costs and a wave propagation model. The maintenance and operation capabilities, and the interactions between devices are also quantified. The whole process was applied to three hypothetical array geometries (*Aligned*, *Staggered* and *Arrow*) in the Gulf of Cádiz (southwestern Spain). Based on the analysis of the results, the following conclusions were drawn:

- The distance between WECs has a significant effect on the potential wave energy: the energy grows with increasing distances. Moreover, the variability between the energy obtained for the individual WECs in the same array is also highly dependent on the separation between WECs: the closer the WECs, the higher the variability. The *Arrow* shape is the most efficient, with improvements up to 20% of the mean energy produced during the life-cycle compared to the other geometries for the same distance between devices.

- The interaction between WECs is also influenced by the separation between them. In the case of the *Aligned* and *Staggered* geometries, the interaction between WECs reduces up to 40% the available resource for the cases of $W = 2D$. However, for the *Arrow* geometry, the interaction is less significant regardless of the distance between devices. For this geometry, all the WECs work under very similar wave conditions, improving the possibilities to be efficiently designed for certain working conditions. Furthermore, the $q-$factor is under 1 for almost all the WECs in every array layout, i.e., the energy production of the nine-WEC array is lower than the production of 9 isolated WECs.

- The efficiency of the different layouts was obtained in terms of potential energy per unit of occupied surface and per unit of maximum width of the facility. Results show that *Aligned* and *Staggered* geometries with

distance between WECs of 2D are the most efficient layouts. However, these geometries present the highest efficiency variabilities when the separation between devices is increased. Distance between devices was found to be a key parameter for efficiency, which decreases with higher distances. For the *Arrow* geometry, the efficiencies are comparatively low, with values up to 90% lower in the case of efficiency per unit of occupied surface and the 6D layout.

- The *Arrow* geometry is the best alternative in terms of maintenance and operation, regardless of the distance between devices. These layouts present the highest availabilities, whereas the differences in the number of wws and the wp between them and the rest of the layouts are negligible. The *Arrow* geometry is only worse in terms of accessibility, as their WECs are exposed to higher waves. Distance between WECs follows the same trends as for the energy performance and efficiency, due to the interaction between WECs. Furthermore, the number of wws and the wp are determined by the wave conditions in the surroundings of the complete facility, rather than the conditions for the approximation of the vessels to the devices.

Acknowledgments

This research was supported by the project 917PTE0538 (CYTED - Programa Iberoamericano de Ciencia y Tecnología para el Desarrollo) and the research group TEP-209 (Junta de Andalucía, `gdfa.ugr.es`). The work of the second author was funded by the Spanish Ministry of Economy and Competitiveness (Research Contract BES-2013-062617).

References

Abanades, J., Greaves, D., Iglesias, G., 2015. Coastal defence using wave farms: The role of farm-to-coast distance. Renewable Energy 75, 572–582. doi:`10.1016/j.renene.2014.10.048`.

Allen, J., Sampanis, K., Wan, J., Greaves, D., Miles, J., Iglesias, G., 2016. Laboratory Tests in the Development of WaveCat. Sustainability 8. doi:`10.3390/su8121339`.

Alonso, R., Solari, S., Teixeira, L., 2015. Wave energy resource assessment in Uruguay. Energy 93, 683–696. doi:`10.1016/j.energy.2015.08.114`.

de Andrés, A., Guanche, R., Meneses, L., Vidal, C., Losada, I., 2014. Factors that influence array layout on wave energy farms. Ocean Engineering 82, 32 – 41. doi:http://dx.doi.org/10.1016/j.oceaneng.2014.02.027.

Babarit, A., 2010. Impact of long separating distances on the energy production of two interacting wave energy converters. Ocean Engineering 37, 718 – 729. doi:http://dx.doi.org/10.1016/j.oceaneng.2010.02.002.

Bergillos, R., López-Ruiz, A., Ortega-Sánchez, M., Masselink, G., Losada, M., 2016. Implications of delta retreat on wave propagation and longshore sediment transport - Guadalfeo case study (southern Spain). Marine Geology 382, 1–16.

Besio, G., Losada, M.A., 2008. Sediment transport patterns at Trafalgar offshore windfarm. Ocean Engineering 35, 653–665. doi:10.1016/j.oceaneng.2008.01.002.

Besio, G., Mentaschi, L., Massino, A., 2015. Wave energy resource assessment in the Mediterranean Sea on the basis of a 35-year hindcast. Energy 94, 50–63. doi:10.1016/j.energy.2015.10.044.

Booij, N., Ris, R.C., Holthuijsen, L.H., 1999. A third-generation wave model for coastal regions 1. Model description and validation. Journal of Geophysical Research 104, 7649–7666. doi:10.1029/98JC02622.

Borgarino, B., Babarit, A., Ferrant, P., 2012. Impact of wave interactions effects on energy absorption in large arrays of wave energy converters. Ocean Engineering 41, 79 – 88. doi:http://dx.doi.org/10.1016/j.oceaneng.2011.12.025.

Bozzi, S., Giassi, M., Moreno Miquel, A., Antonini, A., Bizzozero, F., Gruosso, G., Archetti, R., Passoni, G., 2017. Wave energy farm design in real wave climates: the Italian offshore. Energy 122, 378–389. doi:10.1016/j.energy.2017.01.094.

Budal, K., 1977. Theory for absorption of wave power by a system of interacting bodies. Journal of Ship Research 21, 248–253.

Camus, P., Mendez, F.J., Medina, R., 2011. A hybrid efficient method to downscale wave climate to coastal areas. Coastal Engineering 58, 851–862.

Camus, P., Menéndez, M., Méndez, F.J., Izaguirre, C., Espejo, A., Cánovas, V., Pérez, J., Rueda, A., Losada, I.J., Medina, R., 2014. A weather-type statistical downscaling framework for ocean wave climate. Journal of Geophysical Research C: Oceans 119, 7389–7405.

Cats, G., Wolters, L., 1996. The HIRLAM project. IEEE Computational Science and Engineering 3, 4–7.

Engstrom, J., Eriksson, M., Goteman, M., Isberg, J., Leijon, M., 2013. Performance of large arrays of point absorbing direct-driven wave energy converters. Journal of Applied Physics 114, 204502. doi:10.1063/1.4833241.

Falnes, J., 1980. Radiation impedance matrix and optimum power absorption for interacting oscillators in surface waves. Applied Ocean Research 2, 75 – 80. URL: http://www.sciencedirect.com/science/article/pii/0141118780900322, doi:http://dx.doi.org/10.1016/0141-1187(80)90032-2.

Fernandez, H., Iglesias, G., Carballo, R., Castro, A., Fraguela, J., Taveira-Pinto, F., Sanchez, M., 2012. The new wave energy converter wavecat: Concept and laboratory tests. Marine Structures 29, 58 – 70. doi:http://dx.doi.org/10.1016/j.marstruc.2012.10.002.

Goteman, M., Engstrom, J., Eriksson, M., Isberg, J., Leijon, M., 2014. Methods of reducing power fluctuations in wave energy parks. Journal of Renewable and Sustainable Energy 6, 043103. doi:10.1063/1.4889880.

Guanche, R., de Andrés, A.D., Simal, P.D., Vidal, C., Losada, I.J., 2014. Uncertainty analysis of wave energy farms financial indicators. Renewable Energy 68, 570–580. doi:10.1016/j.renene.2014.02.046.

Iglesias, G., Carballo, R., 2014. Wave farm impact: The role of farm-to-coast distance. Renewable Energy 69, 375–385. doi:10.1016/j.renene.2014.03.059.

Khan, N., Kalair, A., Abas, N., Haider, A., 2017. Review of ocean tidal, wave and thermal energy technologies. Renewable and Sustainable Energy Reviews 72, 590–604. doi:10.1016/j.rser.2017.01.079.

López, I., Andreu, J., Ceballos, S., Martínez De Alegría, I., Kortabarria, I., 2013. Review of wave energy technologies and the necessary power-equipment. Renewable and Sustainable Energy Reviews 27, 413–434. doi:10.1016/j.rser.2013.07.009.

López-Ruiz, A., Bergillos, R.J., Ortega-Sánchez, M., 2016. The importance of wave climate forecasting on the decision-making process for nearshore wave energy exploitation. Applied Energy 182, 191–203. doi:10.1016/j.apenergy.2016.08.088.

Margheritini, L., Vicinanza, D., Frigaard, P., 2009. SSG wave energy converter: Design, reliability and hydraulic performance of an innovative overtopping device. Renewable Energy 34, 1371–1380. doi:10.1016/j.renene.2008.09.009.

Mercadé Ruiz, P., Ferri, F., Kofoed, J., 2017. Experimental Validation of a Wave Energy Converter Array Hydrodynamics Tool. Sustainability 9, 115. doi:10.3390/su9010115.

Ortega-Sánchez, M., Fachin, S., Sancho, F., Losada, M.a., 2008. Relation between beachface morphology and wave climate at Trafalgar beach (Cádiz, Spain). Geomorphology 99, 171–185. doi:10.1016/j.geomorph.2007.10.013.

Pacheco, A., Ferreira, 2016. Hydrodynamic changes imposed by tidal energy converters on extracting energy on a real case scenario. Applied Energy 180, 369–385. doi:10.1016/j.apenergy.2016.07.132.

Reikard, G., Robertson, B., Bidlot, J., 2016. Wave Energy Worldwide: Simulating wave farms, forecasting, and calculating reserves. International Journal of Marine Energy In Review, 156–185. doi:10.1016/j.ijome.2017.01.004.

Rusu, E., Guedes Soares, C., 2013. Coastal impact induced by a Pelamis wave farm operating in the Portuguese nearshore. Renewable Energy 58, 34–49. doi:10.1016/j.renene.2013.03.001.

Veigas, M., Iglesias, G., 2014. Potentials of a hybrid offshore farm for the island of Fuerteventura. Energy Conversion and Management 86, 300–308. doi:10.1016/j.enconman.2014.05.032.

Veigas, M., López, M., Iglesias, G., 2014. Assessing the optimal location for a shoreline wave energy converter. Applied Energy 132, 404–411. doi:10.1016/j.apenergy.2014.07.067.

Vicinanza, D., Margheritini, L., Kofoed, J.P., Buccino, M., 2012. The SSG wave energy converter: Performance, status and recent developments. Energies 5, 193–226. doi:10.3390/en5020193.

Zarzuelo, C., Díez-minguito, M., Ortega-Sánchez, M., López-Ruiz, A., Losada, M.A., 2015. Hydrodynamics response to planned human interventions in a highly diz (Spain) altered embayment : The example of the Bay of Cádiz. Estuarine , Coastal and Shelf Science 167, 1–11. doi:http://dx.doi.org/10.1016/j.ecss.2015.07.010.